Electronic interactions in illuminated carbon dots/MoS_2 ensembles and electrocatalytic activity towards hydrogen evolution

Ruben Canton-Vitoria[a]#, Lorenzo Vallan[b]#, Esteban Urriolabeitía[c], Ana M. Benito[b], Wolfgang K. Maser[b], Nikos Tagmatarchis*[a]

Abstract. We report on the preparation, characterization and photophysical and electrocatalytic properties of carbon dots (CDs)/MoS_2 ensembles. Based on electrostatic interactions, ammonium functionalized MoS_2, prepared upon reaction of 1,2-dithiolane *tert*-butyl carbamate with MoS_2 followed by acidic deprotection, was coupled with CDs bearing multiple carboxylates on their periphery as derived upon microwave-assisted polycondensation of citric acid and ethylenediamine followed by alkaline treatment. Insights into electronic interactions between the two species within CDs/MoS_2 emanated from absorption and photoluminescence titration assays. Efficient fluorescence quenching of CDs by MoS_2 was observed and attributed to photoinduced electron/energy transfer as the decay mechanism for the transduction of the singlet excited state of CDs. Finally, the electrocatalytic performance of CDs/MoS_2 was assessed towards the hydrogen evolution reaction and found superior as compared to that owed to the individual CDs species.

Introduction

One of the most actively investigated 2D materials beyond graphene is arguably MoS_2, which belongs to the larger family of layered transition metal dichalcogenides (LTMDCs).[1] A single layered MoS_2 is a semiconducting pseudo-2D crystal consisting of a metal network sandwiched within two chalcogenide layers, where each metal cation is connected with four chalcogenide anions forming a honeycomb lattice. Bulk LTMDCs can be exfoliated to semiconducting or metallic sheets depending on the exfoliating agents employed. Notably, we recently developed a facile approach leading to exfoliated semiconducting LTMDCs via treatment with chlorosulfonic acid,[2] contrasting the BuLi treatment exfoliation process that gives access predominantly to the metallic polytype structure.[3]

A major drawback of LTMDCs materials is associated with poor solubility, since multiple van der Waals forces between the layers keep them tightly together. Those forces, preventing the separation and individualization of sheets within the LTMDCs, can be overcome by chemical functionalization and the incorporation of species that due to steric and/or electronic reasons may keep apart, by avoiding re-stacking, the sheets of LTMDCs. Hence, functionalization of LTMDCs is imperative for fully harnessing their capabilities and broaden their application in a variety of fields. However, LTMDCs tend to be rather inert – chalcogen atoms in the basal plane are saturated and not highly reactive, while the metal atoms are embedded beneath the chalcogen layer, thus not susceptible to functionalization. Nevertheless, reactions of metallic MoS_2 with organoiodides or diazonium salts yielded MoS_2-based materials carrying organic addends at the basal plane.[4] Moreover, ligand conjugation of thiols to Mo atoms of metallic MoS_2,[5] as a rather debatable route of functionalization, since thiols can convert to the corresponding disulfides in a catalytic reaction activated by the presence of MoS_2, which eventually physisorb onto the basal plane of MoS_2,[6] was also reported. In addition, we recently succeeded the covalent functionalization of exfoliated semiconducting MoS_2, by exploiting the high binding affinity of 1,2-dithiolanes for Mo atoms, particularly those located at the edges of exfoliated semiconducting MoS_2, where S vacancy sites are naturally introduced during the chemical exfoliation from the bulk.[7]

Carbon dots (CDs), since their serendipitously discovery in 2004,[8] proved to be a valuable new entry in the horizon of carbon-based nanomaterials. In general, CDs are nanosized particles, with diameter in the order of 10 nm or less, showing solubility in aqueous and organic media,[9] biocompatibility[10] and photochemical stability.[11] Among the novel physicochemical properties of CDs is their intrinsic photoluminescence,[12] which can be exploited in energy conversion schemes.[13] In particular, photoinduced energy and/or electron transfer processes in CDs have been identified, for example, when combined with carbon nanotubes,[14] graphene oxide,[15] perylene diimides,[16] and porphyrins.[17] Moreover, the high stability and good electrical conductivity of CDs enable them to be considered as interesting contenders for electrocatalysis.[18]

Considering all the above issues, the aim of the current study is three-fold, namely to (i) integrate, by employing electrostatic attractive forces, MoS_2 and CDs possessing opposite charges, into an electron donor-acceptor CDs/MoS_2 system, (ii) scrutinize intra-ensemble electronic interactions

[a] R. Canton-Vitoria, N. Tagmatarchis
Theoretical and Physical Chemistry Institute
National Hellenic Research Foundation
48 Vassileos Constantinou Avenue, 11635 Athens, Greece.
E-mail: tagmatar@eie.gr
[b] L. Vallan, A. M. Benito, W. K. Maser
Instituto de Carboquímica (ICB, CSIC)
Consejo Superior de Investigaciones Científicas
C/Miguel Luesma Castán 4, E-50018 Zaragoza, Spain.
[c] Esteban Urriolabeitía
Instituto de Síntesis Quimica y Catálisis Homogénea
CSIC, Universidad de Zaragoza
C/Pedro Cerbuna 12, E-50009 Zaragoza, Spain
# Equal contribution.

Supporting information for this article is given via a link at the end of the document.

between the two species, and (iii) assess the electrocatalytic performance of CDs/MoS_2 towards the hydrogen evolution reaction (HER). To achieve these goals, semiconducting MoS_2 sheets, as obtained upon wet-exfoliation from the bulk, were functionalized such as to carry positively charged ammonium moieties, and combined with CDs bearing carboxylate anions. Electronic absorption spectroscopy as well as steady-state and time-resolved photoluminescence titration assays were employed to shed light on the electronic communication and the dynamics of the photoinduced processes developed within the CDs/MoS_2 ensembles. Finally, overpotentials and Tafel slopes were evaluated for the assessment of the electrocatalytic activity of CDs/MoS_2 toward the HER.

Results and Discussion

Bulk MoS_2 was exfoliated to semiconducting nanosheets following the chlorosulfonic acid assisted strategy. [2] The exfoliated MoS_2 was spectroscopically evaluated and found to be around 340 nm in lateral size and oligolayered thick.[19] Treatment of exfoliated MoS_2 with the 1,2-dithiolane *tert*-butyl carbamate (BOC) derivative **1**, furnished material **2**, according to Figure 1a. This involves the recently established methodology for the functionalization of chemically-exfoliated LTMDCs, based on the high binding affinity of 1,2-dithiolanes for the Mo atoms, [7] particularly those located at the edges of exfoliated MoS_2. Filtration of the reaction mixture through a PTFE membrane with

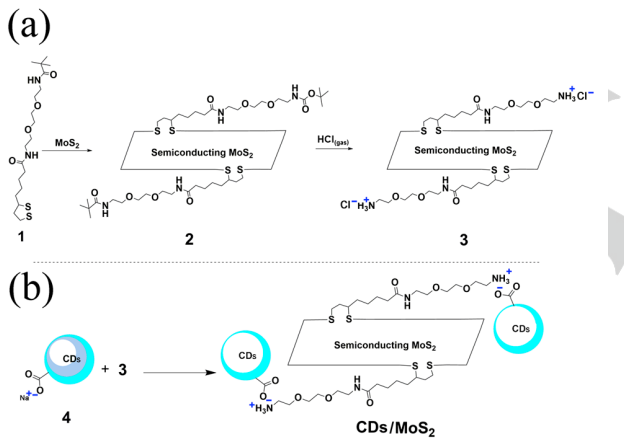

Figure 1. (a) Functionalization of MoS_2 leading to ammonium modified MoS_2-based material **3**. (b) Formation of CDs/MoS_2 ensembles based on electrostatic interactions.

0.2 µm pore size and successive washing with dichloromethane guaranteed that modified MoS_2 material **2** was free of non-covalently associated organic species. The presence of the ethylene glycol side chain in **2** allowed solubility enhancement, tolerating easier handling and manipulation in wet media. Furthermore, the BOC terminating group in **2**, masking the introduced amino-functions, can be easily removed under acidic conditions, yielding ammonium functionalized MoS_2 material **3**.

The chemical transformation was spectroscopically proved by observing alterations in the ATR-IR spectra of materials **2** and **3**. While stretching vibration bands due to C-H units are identified in the region 2800-3000 cm^{-1} for both **2** and **3**, two discrete bands at 1650 and 1710 cm^{-1} owed to carbonyl amide and BOC units, respectively, are present in the IR spectrum of **2**, with the latter band being absent in the spectrum of **3** (Supporting Information, Figure S1), thus justifying the effective BOC-deprotection. Raman spectroscopy revealed the presence of characteristic A_{1g} and E^1_{2g} modes located at 406 and 382 cm^{-1}, respectively, in materials **2** and **3**. Moreover, the A_{1g} and E^1_{2g} modes were found unaltered as compared with the ones present in exfoliated MoS_2 (Supporting Information, Figure S2). Since for exfoliated MoS_2 the calculated frequency difference between A_{1g} and E^1_{2g} is 24 cm^{-1}, corresponding to the presence of 3-4 MoS_2 layers in average,[20] it is reasonable to claim that the same number of layers exists in **2** and **3**. Additionally, no other Raman bands were observed in the region 500-1000 cm^{-1}, indicating the absence of oxidation during the exfoliation and functionalization process, hence, proving the preservation of the electronic properties of the semiconducting MoS_2 polytype. In addition, the ζ-potential value changed from -24 mV for exfoliated MoS_2 to +2.6 mV for **3**, being consistent with the presence of ammonium functionalities. Moreover, Kaiser test revealed a value of 50 µmol/g for free amine units in **3**. Then, based on TGA analysis, the 4.5% mass loss observed during heating of **3** in the temperature range 200-500 °C under nitrogen atmosphere (Supporting Information, Figure S3), related to the decomposition of the organic part incorporated on MoS_2, is consistent with the presence of one functional group for every 49 units of MoS_2. As far as morphology concerns, the MoS_2 material **3** was examined by field-emission SEM. Briefly, a few drops of a methanol dispersion of **3** were deposited onto the sample holder and imaged after the solvent was allowed to slowly evaporate. Polygonal overlapping sheets of MoS_2 with sizes varied between hundreds of nanometers to several micrometers in a random distribution were observed (Supporting Information, Figure S4). Amplification of several areas of the material reveals semi-transparent sheets associated to few layers of MoS_2, with regular and linear edges. It should be pointed out that due to the drying process for imaging, re-staking of the MoS_2 layers occurs explaining not only the deviation observed from the spectroscopically calculated layer size as in solution but also the avoidance of identifying single-layered MoS_2 in the modified material **3**.

In parallel, CDs were synthesized from citric acid and ethylenediamine following a microwave-assisted

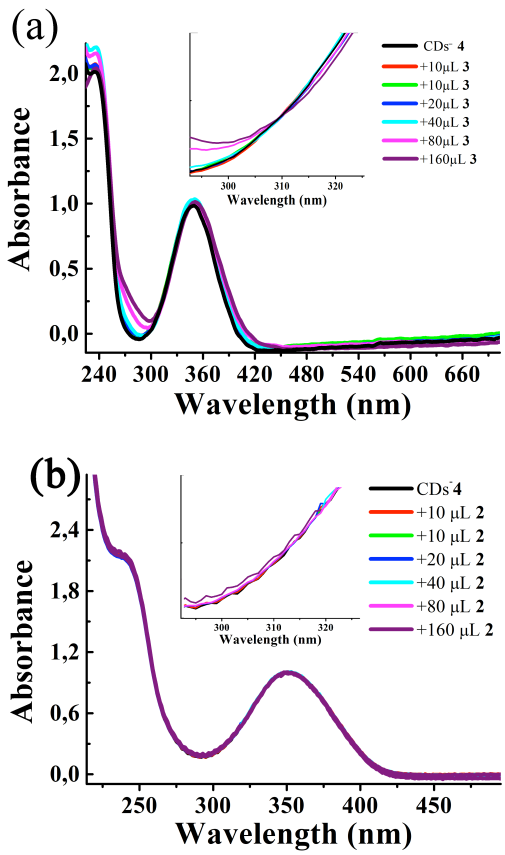

Figure 2. UV-Vis absorption spectra of CDs^- **4** upon incremental additions of (a) ammonium modified MoS_2-based material **3**. Inset: Enlargement of the 300-320 nm region where the isosbestic point is developed, (b) MoS_2-based material **2**.

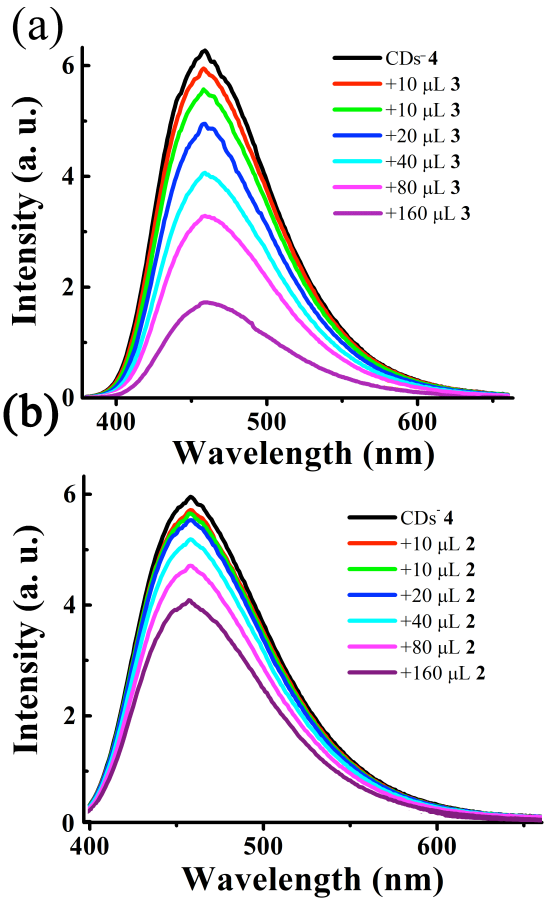

Figure 3. Photoluminescence titration assays of CDs^- **4** (20 μg/mL) upon incremental additions of (a) positively charged MoS_2-based material **3**, and (b) neutral MoS_2-based material **2**. Measurements were conducted in water for samples possessing equal absorbance at the excitation wavelength of 370 nm.

polycondensation method. The microwave irradiation conditions employed guaranteed fast and easy production of 1-2 nm sized fluorescent CDs as revealed by DLS and AFM measurements (Supporting Information, Figure S5), possessing a polyamidic structure with a periphery rich in carboxylic acid moieties as verified by NMR (Supporting Information, Figure S6) and IR assays (Supporting Information, Figure S7). The plethora of –COOH units decorating the surface of the water-soluble CDs can be easily ionized upon addition of aqueous NaOH, giving access to negatively charged CDs^- **4**, which were further purified to remove the excess of NaOH by dialysis (molecular weight cut-off 0.5-1.0 kDa). As far as the optical properties of **4** concerns, they were screened by electronic absorption and photoluminescence spectroscopy. In brief, the UV-Vis spectrum of **4** is governed by two characteristic bands centred at 350 and 230 nm (Supporting Information, Figure S8), while upon 370 nm excitation an emission at 460 nm is identified (Supporting Information, Figure S9).

Next, having in hand modified MoS_2 with positive charges in material **3**, and negatively charged CDs in material **4**, electrostatic attractive interactions between the two species were exploited (Figure 1b) en route the realization of CDs/MoS_2 ensembles. In this direction, a series of aqueous titration assays were conducted. Figure 2 shows the electronic absorption spectra of CDs^- **4** upon addition of incremental amounts of ammonium modified MoS_2 **3**. Subtraction of the MoS_2 absorption background allowed a clear observation of the titration effects – please note that MoS_2 only shows characteristics bands beyond 490 nm, i.e. beyond the absorption bands of CDs^- **4** – and particularly the effect of MoS_2 addition on the CDs^- **4** spectrum – in UV-Vis titration assays without subtracting the MoS_2 bands, the characteristic absorptions of the semiconducting phase of MoS_2 appear at 690, 630 and 490 nm (Supporting Information, Figure S10). Evidently, a progressive red-shift for the absorption of CDs^- **4** is observed, namely from 350 to 355 nm after the addition of 320 μL of **3**. Moreover, a broad isosbestic point at 310 nm, consistent with the complex formation between the two species in the ground state, was developed. Notably, when blank titration assays were conducted, by employing the neutral MoS_2-based derivative **2** instead of the positively charged **3**,

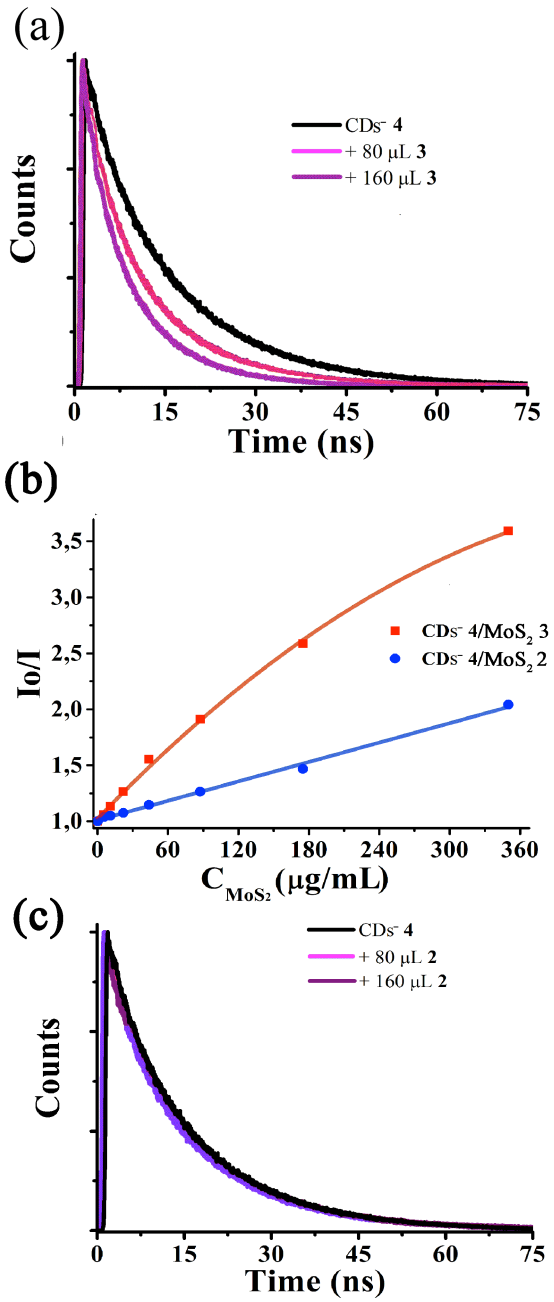

Figure 4. (a) Decay profiles for CDs^- **4** upon incremental additions of positively charged MoS_2-based material **3**. (b) Stern-Volmer plot for the additions of the positively charged MoS_2-based material **3** (red) and the neutral MoS_2-based material **2** (blue) to CDs^- **4**. (c) Decay profiles for CDs^- **4** upon incremental additions of neutral MoS_2-based material **2**.

none of the aforementioned results were observed (Figure 2b), thus, proving the beneficial role of attractive Coulombic forces not only in the establishment of the CDs/MoS_2 ensembles but also on the progression of effective interactions between MoS_2 and CDs.

Meaningful insight on photoinduced electronic interactions between MoS_2 and CDs at the excited states was derived from photoluminescence measurements. Steady-state assays revealed that the 460 nm fluorescence emission of CDs^- **4**, upon excitation at 370 nm, was progressively quenched upon addition of the ammonium modified MoS_2-based material **3** (Figure 3a), for samples possessing equal absorbance at the excitation wavelength. Notably, when blank assays were conducted, by incorporating the neutral MoS_2-based derivative **2** instead of the positively charged **3**, a lower quenching rate for the emission of CDs^- **4** was observed (Figure 3b), ascribed to the inner filter effect of MoS_2. These results suggest strong electronic interactions at the excited states between the positive and negative species within the CDs/MoS_2 ensemble. The photoluminescence quenching is supportive of photoinduced electron and/or energy transfer as the decay mechanism for the transduction of the singlet excited state of CDs.

Next, based on the time-correlated-single-photon-counting method, the fluorescence emission decay profiles for CDs^- **4** were acquired (Figure 4a). The analysis of the decay profiles at 460 nm (excitation at 376 nm) for the singlet excited state of CDs^- **4** was exclusively monoexponentially fitted with a lifetime of 14.0 ns. Addition of the positively charged MoS_2-based material **3** to the negatively charged CDs^- **4** resulted in biexponential fitting, giving rise to the identification of two components, namely, one with the same lifetime, attributed to non-interacting CDs and a faster new one with 3.0 ns lifetime, corresponding to the fluorescence quenching of the emission intensity of the singlet excited state of CDs within the CDs/MoS_2 ensembles. By comparing the lifetime of unbound CDs with the one attributed to the CDs/MoS_2 ensembles, the quenching rate constant k^S_q and the quenching quantum yield Φ^S_q were estimated to be 2.67×10^8 s^{-1} and 0.79, respectively. As a consequence, the photoluminescence ratio I_0/I shows a linear trend for the addition of **2** to CDs^- **4** and a faster as well as non-linear trend for the addition of **3** to CDs^- **4** (Figure 4b), implying that in the latter an additional process takes place, namely, the electrostatic formation of the CDs/MoS_2 ensemble. This is further confirmed upon examination of the fluorescence decay profile for the blank measurement employing neutral MoS_2-based derivative **2**, which remained monoexponentially fitted, following the lifetime of intact CDs^- **4** (Figure 4c).

Finally, the electrocatalytic activity of CDs/MoS_2 towards the hydrogen evolution reaction (HER) was examined by employing a rotating disc working glassy carbon electrode in a standard three-electrode glass cell at a scan rate of 5 mV/sec in 0.5 M H_2SO_4. In general, MoS_2 are promising materials for HER, based on the overpotential and Tafel slope values they exhibit.[21, 22] In addition, the aqueous solubility of CDs together with the presence of surface functional groups contribute to draw hydrated protons, thus enhancing proton adsorption capacity,[23] Based on the above and considering that hydrogen binds too strongly to S, hence leaving as primary active site for MoS_2 the Mo edge, the performance of CDs/MoS_2 towards the HER was probed by linear sweep voltammetry. The polarization curve of CDs/MoS_2 along with those of individual CDs^- **4** and bare glassy carbon electrode for comparison are shown in Figure 5a. For a

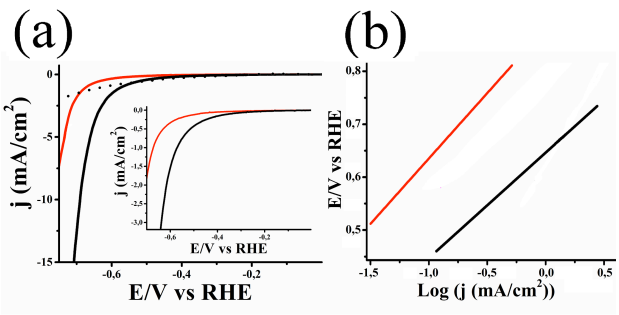

Figure 5. (a) Linear sweep voltammograms for the HER of CDs/MoS_2 (black), individual CDs^- **4** (red) and bare glassy carbon electrode (dotted). Inset: enlarged region near the onset. (b) Tafel plots for CDs/MoS_2 (black) and individual CDs^- **4** (red) showing overpotential vs current density.

given potential, the cathodic current increased for CDs/MoS_2 as compared to that based on individual CDs^- **4** and the bare carbon glassy electrode. The evolution of gaseous hydrogen for CDs/MoS_2 was visualized as bubbles appearing at currents as small as 0.5 mA/cm^2, with enhanced rate at around -0.7 V vs RHE. Since the cathodic current density is proportional to the amount of hydrogen evolved, the latter result highlights the better catalytic activity for CDs/MoS_2 and prominent hydrogen evolution behavior exhibiting an onset overpotential near -0.5 V vs RHE, which is lower than the individual CDs^- **4** by around 150 mV. The better electrocatalytic activity of CDs/MoS_2 is mainly attributed to a synergic effect due to enhanced charge-transfer kinetics owed to the intimate contact between the two species CDs and MoS_2 as well as the presence of active sites in MoS_2. Next, the linear regions of the Tafel plots (Figure 5b) were fit to the Tafel equation, $\eta = B \log j + a$, where η is the overpotential, j is the current density and B is the Tafel slope, to further characterize the fluent charge transport efficiency and the efficacy of the electrocatalytic reaction. Analysis of the Tafel slope helps to elucidate the possible HER mechanism and define the rate-limiting step. The Tafel slope for CDs/MoS_2 ensemble was found to be 22 mV/dec, smaller than that owed to CDs^- **4** by 4 mV/dec. Considering that smaller Tafel slope suggests that for the generation of an equivalent current only a lower overpotential is needed to apply, the electrocatalytic activity of individual CDs^- **4** is improved upon realization of the CDs/MoS_2 ensemble. The latter improvement in charge transport is attributed to good electrical contact between the two components in the donor-acceptor CDs/MoS_2 ensemble, in which charge-transfer phenomena prevail. Moreover, the small Tafel slope of CDs/MoS_2 manifests that the electrochemical desorption of adsorbed hydrogen atoms onto the modified electrode to generate hydrogen is the rate-limiting step – see equations 2 and 3 below. Based on the widely applied mechanisms for the HER, initially a proton is adsorbed onto the electrode surface via a reduction process (Volmer adsorption [Eq. (1)]) followed by either direct bonding of the adsorbed hydrogen atom with another proton and electron transfer from the electrode surface (Heyrovsky desorption [Eq. (2)]) or recombination of two hydrogen atoms adsorbed on the electrode surface (Tafel desorption [Eq. (3)]).

Volmer adsorption: $H^+ + e^- \rightarrow H^{\bullet}_{(ads)}$ (1)

Heyrovsky desorption: $H^{\bullet}_{(ads)} + H^+ + e^- \rightarrow H_2$ (2)

Tafel desorption: $H^{\bullet}_{(ads)} + H^{\bullet}_{(ads)} \rightarrow H_2$ (3)

Conclusions

We developed aqueous stable CDs/MoS_2 ensembles, in which the two components are tightly held together in a controlled fashion by electrostatic interactions. Electronic absorption and photoluminescence titration assays, complemented by time-resolved fluorescence emission, unambiguously proved the formation of the ensembles and the electronic interplay within them. Significant quenching of the CDs centred photoluminescence by MoS_2 was revealed, prompting to an additional deactivation channel – electron and/or energy transfer – starting from the singlet excited state of CDs within the CDs/MoS_2 ensembles. Moreover, the electrocatalytic performance of CDs/MoS_2 was evaluated regarding the HER and found improved in comparison with that of the individual CDs species. Without a doubt, such CDs/MoS_2 ensembles performing in electron donor-acceptor schemes can be further exploited for managing charge-transfer processes as well as for electrocatalysis and may be useful for advancing the field of energy conversion in a wide range of technological and environmental applications.

Experimental Section

Instrumentation. Steady-state UV-Vis electronic absorption spectra were recorded on a PerkinElmer (Lambda 19) UV-Vis-NIR spectrophotometer. Steady-state emission spectra were recorded on a Fluorolog-3 JobinYvon-Spex spectrofluorometer (model GL3-21). Picosecond time-resolved fluorescence spectra were measured by the time-correlated-single-photon-counting (TCSPC) method on a Nano-Log spectrofluorometer (Horiba JobinYvon), by using a laser diode as an excitation source (NanoLED, 375 nm) and a UV-Vis detector TBX-PMT series (250-850 nm) by Horiba JobinYvon. Lifetimes were evaluated with the DAS6 Fluorescence-Decay Analysis Software. Mid-infrared spectra in the region 500−4500 cm^{-1} were obtained on a Fourier transform IR spectrometer (Equinox 55 from Bruker Optics) equipped with a single reflection diamond ATR accessory (DuraSamp1IR II by SensIR Technologies). A drop of the solution was placed on the diamond surface, followed by evaporation of the solvent, in a stream of nitrogen, before recording the spectrum. Typically, 100 scans were acquired at 2 cm^{-1} resolution. Micro-Raman scattering measurements were performed at room temperature in the backscattering geometry using a RENISHAW inVia Raman microscope equipped with a CCD camera and a Leica microscope. A 2400 lines mm^{-1} grating was used for all measurements, providing a spectral resolution of ± 1 cm^{-1}. As an excitation source the Ar^+ laser (514 nm with less than 0,092 mW laser power) was used. Measurements were taken with 15 seconds of exposure times at varying numbers of accumulations. The laser spot was focused on the sample surface using a long working distance 50x objective. Raman spectra were collected on numerous spots on the sample and recorded with Peltier cooled CCD camera. The data were collected and analyzed with Renishaw Wire and Origin software. Thermogravimetric analysis was performed using a TGA Q500 V20.2 Build 27 instrument by TA in a nitrogen (purity >99.999%) inert atmosphere. The microwave-assisted

reaction was performed in a CEM Discover SP reactor employed in open-batch modality. Atomic force microscopy (AFM) images were acquired in air under ambient conditions using a MultiMode AFM with NanoScope V controller (Bruker Nano Surfaces Division, Santa Barbara, CA) operating in tapping mode with Si tips Bruker AFM probe RTESPA PART MPP-11120-10. Samples were prepared on mica substrates. Particle height distribution analysis was carried out by using the Nanoscope Analysis Version 1.5 software (Veeco Ins). Elemental analyses were performed in a Thermo Flash EA 1112 instrument with ~3 mg of powder samples. The DLS measurements were recorded on a Malvern Nano Zetasizer HT, on a 10 mm path-length plastic cuvette. ^{1}H and ^{13}C NMR spectra were recorded in D_2O solutions at 25 ^{o}C on a Bruker AV500 spectrometer. Electrochemical measurements were carried out at room temperature in N_2-saturated 0.5 M H_2SO_4 in a standard three-compartment electrochemical cell using an EG&G Princeton Applied Research potensiostat/galvanostat (Model PARSTAT^{R} 2273A). As counter electrode, a platinum wire was used and as reference a $Hg/HgSO_4$ (0.5 M K_2SO_4) electrode was placed into Luggin capillary. The working electrode was a glassy carbon disk with geometric surface area of 0.071 cm^2. Linear sweep voltammetry measurements were conducted with a scan rate of 5 mV s^{-1}.

Synthesis of carbon dots. 2.0 g of citric acid monohydrate (9.5 mmol) were dissolved in 16 mL of ultrapure water. Upon addition of 0.64 mL of ethylenediamine (9.5 mmol) the solution was heated up through microwave irradiation. The mixture was irradiated in order to keep the temperature at 140°C for 6 minutes, after that the irradiation was stopped. This yields in a yellow, transparent solid product, highly soluble in water. The product was dissolved in ultrapure water and dialyzed against ultrapure water (MWCO = 0.5-1.0 KDa, 3 days, twice a day). The dry material CDs^{-} **4** was obtained by freeze-drying, with a yield in mass of 22 wt. %.

Preparation of MoS_2-based materials 2 and 3. In a round bottom flask, exfoliated MoS_2 (35 mg) and 1,2-dithiolane derivative **1** (15 mg) in DMF (10 mL) were stirred at 70 °C for 40 hours. After that period, the reaction mixture was filtered through a PTFE membrane (0.2 µm pore size), the solid residue was extensively washed with DMF and dichloromethane to obtain material **2**. Then, 15 mg of **2** were redisperse in dichloromethane and treated with gaseous HCl for 2 minutes. The reaction mixture was left under stirring for 12 hours and then filtered through a PTFE membrane (0.2 µm pore size). The solid residue was extensively washed with DMF and dichloromethane to obtain the ammonium derivatized MoS_2-based material **3**.

Acknowledgements

This project has received funding from the European Union's Horizon 2020 research and innovation programme under the Marie Sklodowska-Curie grant agreement N^{o} 642742.

Keywords: MoS_2 • carbon dots • donor-acceptor • hydrogen evolution reaction • energy conversion

[1] (a) X. Huang, Z. Zenga, H. Zhang, *Chem. Soc. Rev*. **2013**, *42*, 1934; (b) M. Pumera, Z. Sofer, A. Ambrosi, *J. Mater. Chem. A* **2014**, *2*, 8981.

[2] G. Pagona, C. Bittencourt, R. Arenal, N. Tagmatarchis, *Chem. Commun.* **2015**, *51*, 12950.

[3] (a) J. Zheng, H. Zhang, S. Dong, Y. Liu, C. T. Nai, H. S. Shin, H. Y. Jeong, B. Liu, K. P. Loh, *Nature Commun.* **2014**, *5*, 2995; (b) Y. Yao, L. Tolentino, Z. Yang, X. Song, W. Zhang, Y. Chen, C.-P. Wong, *Adv. Funct. Mater.* **2013**, *23*, 3577; (c) G. Eda, H. Yamaguchi, D. Voiry, T. Fujita, M. Chen, M. Chhowalla, *Nano Lett.* **2011**, *11*, 5111; (d) Z. Zeng, Z. Yin, X. Huang, H. Li, Q. He, G. Lu, F. Boey, H. Zhang, *Angew. Chem. Int. Ed.* **2011**, *50*, 11093.

[4] (a) D. Voiry, A. Goswami, R. Kappera, C. d. C. C. Silva, D. Kaplan, T. Fujita, M. Chen, T. Asefa, M. Chhowalla, *Nature Chem.* **2015**, *7*, 45; (b) K. C. Knirsch, N. C Berner, H. C. Nerl, C. S. Cucinotta, Z. Gholamvand, N. McEvoy, Z. Wang, I. Abramovic, P. Vecera, M. Halik, S. Sanvito, G. S. Duesberg, V. Nicolosi, F. Hauke, A. Hirsch, J. N. Coleman, C. Backes, *ACS Nano* **2015**, *9*, 6018.

[5] (a) S. S. Chou, M. De, J. Kim, S. Byun, C. Dykstra, J. Yu, J. Huang, V. P. Dravid, *J. Am. Chem. Soc.* **2013**, *135*, 4584; (b) L. Zhou, B. He, Y. Yang, Y. He, *RSC Adv*. **2014**, *4*, 32570; (c) R. Anbazhagan, H.-J. Wang, H.-C. Tsai, R.-J. Jeng, *RSC Advances* **2014**, *4,* 42936; (d) J.-S. Kim, H.-W. Yoo, H. O. Choi, H.-T. Jung, *Nano Lett.* **2014,** *14*, 5941; (e) T. Liu, S. Shi, C. Liang, S. Shen, L. Cheng, C. Wang, X. Song, S. Goel, T. E. Barnhart, W. Cai, Z. Liu, *ACS Nano* **2015**, *9*, 950; (f) E. P. Nguyen, B. J. Carey, J. Z. Ou, J. van Embden, E. D. Gaspera, A. F. Chrimes, M. J. S. Spencer, S. Zhuiykov, K. Kalantar-zadeh, T. Daeneke, *Adv. Mater.* **2015**, *27,* 6224; (g) K. Cho, M. Min, T.-Y. Kim, H. Jeong, J. Pak, J.-K. Kim, J. Jang, S. J. Yun, Y. H. Lee, W.-K. Hong, T. Lee, *ACS Nano* **2015**, *9*, 8044.

[6] X. Chen, N. C. Berner, C. Backes, G. S. Duesberg, A. R. McDonald*, Angew. Chem. Int. Ed.* **2016**, *55*, 5803.

[7] R. Canton-Vitoria, Y Sayed-Ahmad-Baraza, M. Pelaez-Fernandez, R. Arenal, C. Bittencourt, C. P. Ewels, N. Tagmatarchis, *NPJ 2D Mater. Appl.* **2017**, *1*, 13.

[8] X. Xu, R. Ray, Y. Gu, H. J. Ploehn, L. Gearheart, K. Raker, W. A. Scrivens, *J. Am. Chem. Soc.* **2004**, *126*, 12736.

[9] J. Gu, D. Hu, J. Huang, X. Huang, Q. Zhang, X. Jia, K. Xi, *Nanoscale* **2016**, *8*, 3973.

[10] (a) A. N. Emam, S. A. Loutfy, A. A. Mostafa, H. Awad, M. B. Mohamed, *RSC Advances* **2017**, *7*, 23502; (b) Y. Sun, W. Cao, S. Li, S. Jin, K. Hu, L. Hu, Y. Huang, X. Gao, Y. Wu, X. J. Liang, *Sci. Rep.* **2013**, *3*, 3036.

[11] K. K. R. Datta, G. Qi, R. Zboril, E. P. Giannelis, *J. Mater. Chem. C* **2016**, *4*, 9798.

[12] S. N. Baker, G. A. Baker*, Angew. Chem. Int. Ed.* 2010, **49**, 6726.

[13] (a) B. C. M. Martindale, E. Joliat, C. Bachmann, R. Alberto, E. Reisner, *Angew. Chem. Int. Ed.* **2016**, *55*, 9402; (b) J. T. Margraf, F. Lodermeyer, V. Strauss, P. Haines, J. Walter, W. Peukert, R. D. Costa, T. Clark, D. M. Guldi, *Nanoscale* Horiz. **2016**, *1*, 220; (c) X. Li, M. Rui, J. Song, Z. Shen, H. Zeng*, Adv. Funct. Mater.* **2015**, *25*, 4929; (d) B. C. M. Martindale, G. A. M. Hutton, C. A. Caputo, E. Reisner, *J. Am. Chem. Soc.* **2015**, *137*, 6018; (e) W. Kwon, G. Lee, S. Do, T. Joo, S. W. Rhee, *Small* **2014**, *10*, 506.

[14] (a) V. Strauss, J. T. Margraf, T. Clark, D. M. Guldi*, Chem. Sci.* **2015**, 6, 6878; (b) T. Skaltsas, A. Stergiou, D. D. Chronopoulos, S. Zhao, H. Shinohara, N. Tagmatarchis*, J. Phys. Chem. C* **2016**, *120*, 8550.

[15] P. Yu, X. Wen, Y.-R. Toh, Y.-C. Lee, K.-Y. Huang, S. Huang, S. Shrestha, G. Conibeer, J. Tang, *J. Mater. Chem. C* **2014**, *2,* 2894.

[16] V. Strauss, J. T. Margraf, K. Dirian, Z. Syrgiannis, M. Prato, C. Wessendorf, A. Hirsch, T. Clark, D. M. Guldi, *Angew. Chem. Int. Ed.* **2015**, *54*, 8292.

[17] F. Arcoudi, V. Strauss, L. Dordevic, A. Cadranel, D. M. Guldi, M. Prato, *Angew. Chem. Int. Ed.* **2017**, *56*, 12097.

[18] (a) Y. Wang, A. Hu, *J. Mater. Chem. C* **2014**, *2*, 6921; (b) Y. Du, S. Guo, *Nanoscale* **2016**, *8*, 2532.

[19] C. Backes, R. J. Smith, N. McEvoy, N. C. Berner, D. McCloskey, H. C. Nerl, A. O'Neill, P. J. King, T. Higgins, D. Hanlon, N. Scheuschner, J. Maultzsch, L. Houben, G. S. Duesberg, J. F. Donogan, V. Nicolosi, J. N. Coleman, *Nat. Comm*. **2014** *5*, 4576.

[20] (a) H. Li, Q. Zhang, C. C. R. Yap, B. K. Tay, T. H. T. Edwin, A. Olivier, D. Baillargeat, *Adv. Funct. Mater.* **2012**, *22*, 1385; (b) S.-L. Li, H. Miyazaki, H. Song, H. Kuramochi, S. Nakaharai , K. Tsukagoshi, *ACS Nano* **2012**, *6*, 7381.

[21] X. Chia, A. Y. S. Eng, A. Ambrosi, S. M. Tan, M. Pumera, *Chem. Rev*. **2015**, *115*, 11941

[22] (a) T. F. Jaramillo, K. P. Jørgensen, J. Bonde, J. H. Nielsen, S. Horch, I. Chorkendorff, *Science* **2007**, *317*, 100; (b) J. Kibsgaard, Z. Chen, B. N. Reinecke, T. F. Jaramillo, *Nature Mater*. **2012**, *11*, 963; (c) Y. Li, H. Wang, L. Xie, Y. Liang, G. Hong, H. Dai, *J. Am. Chem. Soc*. **2011**, *133*, 7296; (d) D. Voiry, M. Salehi, R. Silva, T. Fujita, M. Chen, T. Asefa, V. B. Shenoy, G. Eda, M. Chhowalla, *NanoLett*. **2013**, *13*, 6222.

[23] H. Li, J. Liu, S. J. Guo, Y. L. Zhang, H. Huang, Y. Liu and Z. H. Kang, *J. Mater. Chem. B* **2015**, *3*, 2378.

Entry for the Table of Contents

FULL PAPER

Aqueous stable CDs/MoS_2 ensembles were developed by electrostatic interactions. The efficient photoluminescence quenching of CDs by MoS_2 together with the improved electrocatalytic performance of CDs/MoS_2 towards the HER will be employed to advance the field of energy conversion applications.

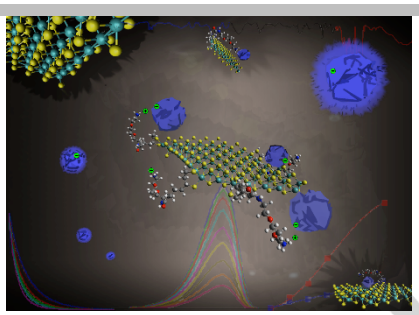

Ruben Canton-Vitoria[a]#, Lorenzo Vallan[b]#, Esteban Urriolabeitia[c], Ana M. Benito[b], Wolfgang K. Maser[b], Nikos Tagmatarchis[a]*

Page No. – Page No.

Electronic interactions in illuminated carbon dots/MoS_2 ensembles and electrocatalytic activity towards hydrogen evolution